JPE 6-1-4

Sensorless Control for a PM Synchronous Motor in a Single Piston Rotary Compressor

Kwan-Yuhl Cho†

†Department of Information and Control Engineering, Chungju National University, Chungbuk, Korea

ABSTRACT

A sensorless control for an IPM (Interior Permanent Magnet) synchronous motor in a single piston rotary compressor is presented in this study. The rotor position is estimated from the d-axis and q-axis current errors between the real system and a motor model of the position estimator. The torque pulsation of the single piston rotary compressor is compensated to reduce speed ripples, as well as, mechanical noise and vibration. The proposed sensorless drive enables the compressor to operate at a lower speed which increases energy savings and reduces mechanical noise. It also gives high speed operations by a flux weakening control for rapid air-cooling and heating of the heat pump air-conditioners.

Keywords: PMSM, sensorless drive, rotary compressor, torque compensation

1. Introduction

PM synchronous motors with variable speed drives have been applied to home appliance products including air-conditioners, refrigerators, and washers to reduce power consumption and acoustic noise, as well as, to provide a more comfortable home environment. In the case of heat pump air-conditioners, wide variable speed operation is required, that is, low speed operation for high efficiency and low acoustic noise, high speed operation for rapid air-cooling and heating. Recently, a single piston rotary compressor with concentrated winding in a PM synchronous motor has become a hot issue in reducing manufacturing costs of air conditioners. Single piston rotary compressors at low speeds, however, have serious mechanical vibrations caused by large torque pulsations during suction, compression, and discharging, as shown in Fig. 1. The peak torque of a single piston rotary compressor at compression reaches about 2.7 times the average load torque.

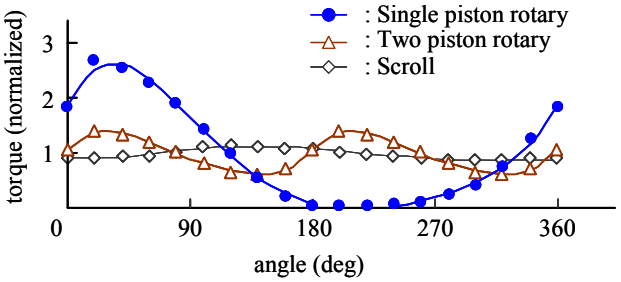

Fig. 1 Torque patterns of rotary and scroll compressors

Fig. 2 shows the structure of the PM synchronous motor with distributed winding and concentrated winding. Line to line inductance and phase back EMF waveforms of the concentrated winding PM synchronous motor are shown in Fig. 3. The stator teeth for the concentrated windings of

Manuscript received October 4, 2005; revised November 1, 2005
†Corresponding Author: kycho@mail.chungju.ac.kr
Tel: +82-43-841-5329, Fax: +82-43-841-5320, Chungju Nat'l Univ.

a PM synchronous motor, which is similar to those of the switched reluctance motor, reduces manufacturing costs and also decreases copper losses of the stator windings due to its short end coils compared with distributed windings. Concentrated windings, however, have serious mechanical vibration and acoustic noise due to the deformation of the stator teeth caused by the concentrated forces [1-3].

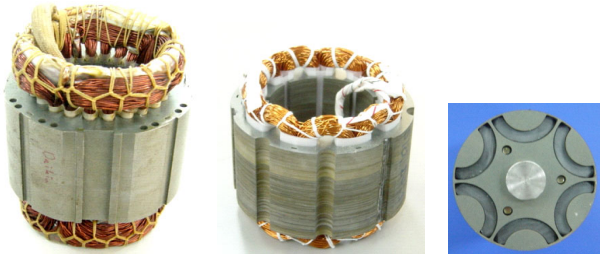

(a) (b) (c)

Fig. 2 Configuration of PM synchronous motors
(a) Distributed winding
(b) Concentrated winding
(c) Rotor with interior permanent magnet

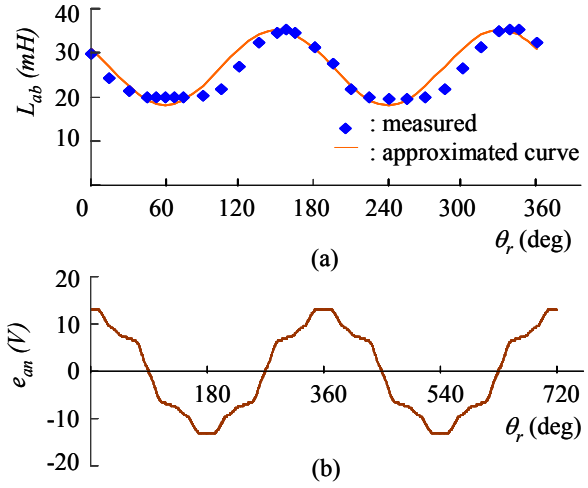

Fig. 3 Inductance and back emf waveforms
(a) Line to line inductance
(b) Back emf at 600rpm

For drive systems of PM synchronous motor compressors, a sensorless control without a mechanical position sensor is required due to the high temperatures and high pressures in the shell of the compressors. The phase current of the PM synchronous motor can be applied as rectangular waveforms and sinusoidal waveforms according to the waveforms of back-EMFs[4-7]. Sensorless controls with rectangular current waveforms, where the commutation periods are determined from the induced voltage of the open phases, have been generally applied due to its simple control strategy. But, it has high acoustic noise and mechanical vibrations due to large commutation torque ripples. Furthermore, its maximum torque per ampere operation and high speed operations, particularly for interior PM synchronous motors, is limited due to the restricted lead angles available. For example, the advanced angle of the phase voltage that leads back to the EMF can not exceed 30 degrees when the commutation signal is detected by the zero-crossing of the open phase back-EMFs. In this paper, a sensorless drive with sinusoidal current waveforms for an interior PM synchronous motor is proposed. For wide variable speed operations, torque control with feed-forward torque compensation at low speeds and flux weakening control at high speeds are also presented.

2. Sensorless Control of PMSM

2.1 Rotor position detecting algorithm

The interior PM synchronous motor, where the permanent magnets are inserted in the rotor core, can be modeled in the rotor reference frame for convenient analysis, speed and current controller design. The *dq*-axis is based on the real rotor position θ_r and the γδ-axis is based on the estimated rotor position θ_M. Both are shown in Fig. 4.

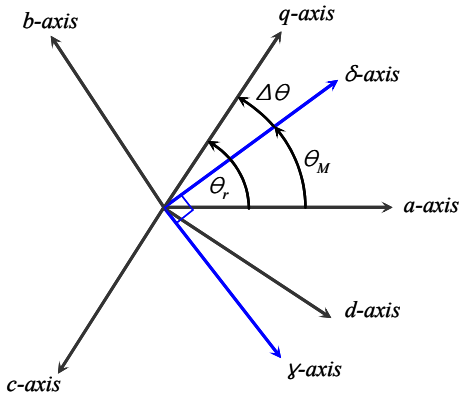

Fig. 4 Axis of rotation

The q-axis leads the a-axis by θ_r and the estimated δ-axis leads the a-axis by θ_M. The d-axis and γ-axis are perpendicular to the q-axis and δ-axis, respectively. The voltage equation of a PM synchronous motor in the dq reference frame can be expressed by (1),

$$\begin{bmatrix} v_d \\ v_q \end{bmatrix} = \begin{bmatrix} r_s + L_d p & -\omega_r L_q \\ \omega_r L_d & r_s + L_q p \end{bmatrix} \begin{bmatrix} i_d \\ i_q \end{bmatrix} + e \begin{bmatrix} 0 \\ 1 \end{bmatrix} \tag{1}$$

where $e=\phi_f\omega_r$ is the back-EMF of the actual motor. Similarly, the voltage equation in the estimated $\gamma\delta$ reference frame can be expressed by (2),

$$\begin{bmatrix} v_\gamma \\ v_\delta \end{bmatrix} = \begin{bmatrix} r_s + L_d p & -\omega_M L_q \\ \omega_M L_d & r_s + L_q p \end{bmatrix} \begin{bmatrix} i_\gamma \\ i_\delta \end{bmatrix} + e \begin{bmatrix} -\sin\Delta\theta \\ \cos\Delta\theta \end{bmatrix} \tag{2}$$

where $\Delta\theta = \theta_r - \theta_M$. From (1) and (2), the rotor position and speed can be estimated by using the current errors between the actual current and model current based on the estimated rotor position. The current model of the PM synchronous motor can be rearranged by (3) from (2),

$$p \begin{bmatrix} i_\gamma \\ i_\delta \end{bmatrix} = \begin{bmatrix} -\frac{r_s}{L_d} & \frac{L_q}{L_d}\omega_M \\ -\frac{L_d}{L_q}\omega_M & -\frac{r_s}{L_q} \end{bmatrix} \begin{bmatrix} i_\gamma \\ i_\delta \end{bmatrix} + \begin{bmatrix} \frac{v_\gamma}{L_d} \\ \frac{v_\delta}{L_q} \end{bmatrix} - e \begin{bmatrix} -\frac{\sin\Delta\theta}{L_d} \\ \frac{\cos\Delta\theta}{L_q} \end{bmatrix} \tag{3}$$

The current dynamic model of (3) precisely gives the same dynamics of the real system given in (1), although two base axes of the rotor position are different. The model given in (3) can be expressed in the discrete form of (4), assuming the motor speed is constant during the sampling time T, which is short compared with the time constant of the current and speed dynamics.

$$\begin{bmatrix} i_\gamma(n+1) \\ i_\delta(n+1) \end{bmatrix} = \begin{bmatrix} 1-\frac{r_s}{L_d}T & -\frac{L_q}{L_d}\omega_M T \\ \frac{L_d}{L_q}\omega_M T & 1-\frac{r_s}{L_q}T \end{bmatrix} \begin{bmatrix} i_\gamma(n) \\ i_\delta(n) \end{bmatrix} + \begin{bmatrix} \frac{T}{L_d}v_\gamma(n) \\ \frac{T}{L_q}v_\delta(n) \end{bmatrix} - e(n) \begin{bmatrix} -\frac{T}{L_d}\sin\Delta\theta(n) \\ \frac{T}{L_q}\cos\Delta\theta(n) \end{bmatrix} \tag{4}$$

To derive a model for the estimation of the rotor position and speed, the current of the next sampling time in the model of the position estimator can be given by (5)

$$\begin{bmatrix} i_{\gamma M}(n+1) \\ i_{\delta M}(n+1) \end{bmatrix} = \begin{bmatrix} 1-\frac{r_s}{L_d}T & -\frac{L_q}{L_d}\omega_M T \\ \frac{L_q}{L_d}\omega_M T & 1-\frac{r_s}{L_q}T \end{bmatrix} \begin{bmatrix} i_\gamma(n) \\ i_\delta(n) \end{bmatrix} + \begin{bmatrix} \frac{T}{L_d}v_\gamma(n) \\ \frac{T}{L_q}v_\delta(n) \end{bmatrix} - e_M(n) \begin{bmatrix} 0 \\ \frac{T}{L_q} \end{bmatrix} \tag{5}$$

In the model of the estimator given by (5), the γδ-axis back-EMFs are assumed to have no phase delay compared with those of the real system, where, the magnitude of δ-axis back-EMFs of the estimator and real system are different. This implies that the γδ-axis back-EMFs of the estimator may represent precisely those of the real system if the rotor position of the estimator is able to track the real rotor position. The current errors between the actual currents and model currents can be given by (6) from (4) and (5)

$$\begin{aligned} \begin{bmatrix} \Delta i_{\gamma M}(n+1) \\ \Delta i_{\delta M}(n+1) \end{bmatrix} &= \begin{bmatrix} i_\gamma(n+1) - i_{\gamma M}(n+1) \\ i_\delta(n+1) - i_{\delta M}(n+1) \end{bmatrix} \\ &= \begin{bmatrix} \frac{T}{L_d}e\sin\Delta\theta \\ \frac{T}{L_q}(e_M - e\cos\Delta\theta) \end{bmatrix} = \begin{bmatrix} \frac{T}{L_d}e\Delta\theta \\ -\frac{T}{L_q}(e - e_M) \end{bmatrix} \end{aligned} \tag{6}$$

In equation (6), $\cos\Delta\theta$ and $\sin\Delta\theta$ can be approximated as $\cos\Delta\theta \approx 1$, $\sin\Delta\theta \approx \Delta\theta$ for small $\Delta\theta$. It is noted from (6) that the difference in the back-EMFs between the real system and estimator depends on the δ-axis current error. While the estimated position error depends on the γ-axis current error. Therefore, the difference of the back-EMF and rotor position between the real system and estimator can be calculated by (7) and (8), respectively

$$\delta e(n) = -k_e \Delta i_\delta(n) \tag{7}$$

$$\delta\theta(n) = k_\theta \Delta i_\gamma(n) \tag{8}$$

where k_e and k_θ are the back-EMF estimation gain and phase estimation gain of the estimator, respectively. Using (7) and (8), the estimated back-EMF and rotor position can be expressed by (9) and (10), respectively

$$e_M(n+1) = e_M(n) + \delta e(n) = e_M(n) - k_e \Delta i_\delta(n) \quad (9)$$

$$\theta_M(n+1) = \theta_M(n) + \frac{T}{\phi_f} e_M(n+1) + \delta\theta(n)$$
$$= \theta_M(n) + \frac{T}{\phi_f} e_M(n+1) + \mathrm{sgn}(\omega_M(n)) \cdot k_\theta \Delta i_\gamma(n) \quad (10)$$

As given in (10), the propagation of the rotor position between sampling periods is mainly activated by the back-EMF at normal operating conditions. The estimated rotor speed can be derived by filtering position propagation during sampling periods and is given by (11),

$$\omega_M(n+1) = [\theta_M(n+1) - \theta_M(n)]/T \quad (11)$$

Current errors between the real system and the model of the estimator make the estimated rotor position tracks the real rotor position. The convergence of the estimated rotor position to the actual rotor position depends on the EMF estimation gain (k_q) and the phase estimation gain (k_d). To increase the motor speed rapidly at low speeds, the EMF estimation gain and the phase estimation gain are inversely proportional to the motor speeds.

2.2 Optimal current trajectory and flux weakening control

The electromagnetic torque of a PM synchronous motor consists of magnetic torque and reluctance torque. The reluctance torque of a SPM synchronous motor is zero due to equal *d*-axis and *q*-axis inductances. For an IPM synchronous motor, however, the difference between *d*-axis inductance and *q*-axis inductance generates the reluctance torque; so that the current should have phase leading to the back-EMF to maximize the total electromagnetic torque. The electromagnetic torque can be expressed as (12),

$$T_e = \frac{3}{2}\frac{P}{2}\{\phi_f i_q + (L_d - L_q) i_d i_q\} \quad (12)$$

where ϕ_f is the back-EMF constant. The optimal *d*-axis and *q*-axis currents for maximum torque/ampere operation depend on the load torque, *d*-axis and *q*-axis inductances. For a given load torque, the relationship between the *d*-axis current and *q*-axis current can be expressed as (13),

$$i_d^* = a_o - \sqrt{a_o^2 + i_q^{*2}} \quad (13)$$

where $a_o = \phi_f / (2 \cdot (L_q - L_d))$

Fig. 5 shows the optimal current trajectory for some load torques and the relationship between current magnitude and current lead angles. Two methods for maximum torque/ampere operation may be considered. First, the reference torque which was generated from the speed controller makes the *q*-axis current reference. Whereas the *d*-axis current reference is generated by the *q*-axis current reference as given in (13). In the second method, the reference torque generates the magnitude of the current. The *d*-axis and *q*-axis currents are generated from the magnitude of current and lead angles, as shown in Fig. 5(b). In this paper, the second method is applied.

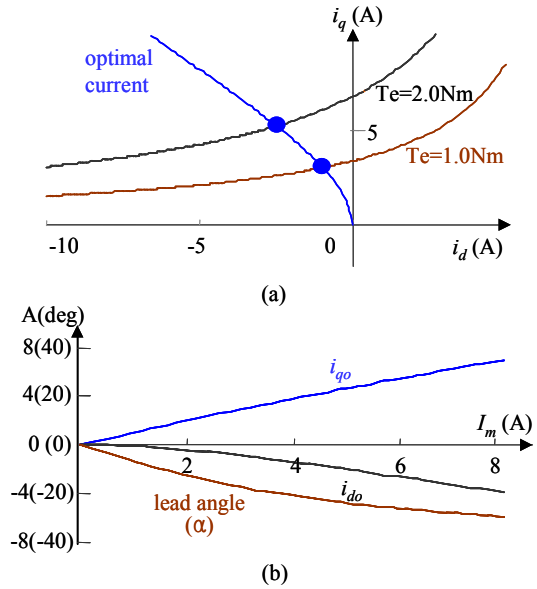

Fig. 5 Optimal current trajectory
(a) Optimal d-axis and q-axis current
(b) Optimal current and lead angle

As the motor speed increases and reaches a certain speed, the optimal current can not be applied to the motor due to the increased back-EMF voltage. In this case, the optimal current trajectory should be replaced by another current trajectory, such as flux weakening. The voltage

equations for an IPM synchronous motor at steady state may be given as

$$V_{qs} = r_s i_{qs} + \omega_r L_d i_{ds} + \phi_f \omega_r$$
$$V_{ds} = r_s i_{ds} - \omega_r L_q i_{qs} \quad (14)$$

The *d*-axis and *q*-axis voltages are limited by the available maximum output voltage of the inverter, which is given by

$$V_{qs}^{\ 2} + V_{ds}^{\ 2} \le V_{\max}^{\ 2} \quad (15)$$

where the maximum voltage V_{max} depends on the DC link voltage and PWM characteristics, including dead time compensation. The available *q*-axis and *d*-axis currents under the voltage limit condition can be expressed by (16) from (14) and (15), where the resistance voltage drop can be neglected at high speeds,

$$i_{qs}^{\ 2} + (i_{ds} + \frac{\phi_f}{L_d})^2 \le (\frac{V_{\max}}{\omega_r L_q})^2 \quad (16)$$

Fig. 6(a) shows the available current regions with motor speeds. As the motor speed increases, the available current region becomes smaller. For a load torque of 1.5Nm, the motor operates at the maximum torque/ampere region up to 4,800rpm. However, the motor speed can not be increased any more by optimal current, i_{do} and i_{qo}. The motor speed can be elevated by adding extra *d*-axis current and decreasing the *q*-axis current. Fig. 6(b) shows the boundary curve between the maximum torque/ampere region and the flux weakening region. Boundary curve depends on load torque and motor speed. For a load torque of 2Nm, the maximum speed for maximum torque/ampere operation is about 4,700rpm and can be reached at 7,000 rpm by a flux weakening control. In this stage, one problem must be considered, that is, mode change from maximum torque/ampere operating mode to flux weakening mode. As shown in Fig. 6(b), the mode change condition can be determined by considering the motor speed, load torque. In this method, the mode change condition is affected by variations of the DC link voltage and motor parameters including stator resistance and back-EMF constant. To avoid such dependency on motor parameters, in this paper, mode change condition is determined by the PWM duty of the phase voltage. Along with optimal current trajectory, PWM duty increases as the motor speed increases. The operating mode changes from a flux weakening region to a maximum torque/ampere region when the PWM duty in the voltage controller reaches full duty, as in space vector modulation. When the operating mode enters the flux weakening mode, the extra *d*-axis current is added to the *d*-axis current reference; however, *q*-axis current reference should be reduced. The extra *d*-axis current for flux weakening can be determined by speed errors through PI control.

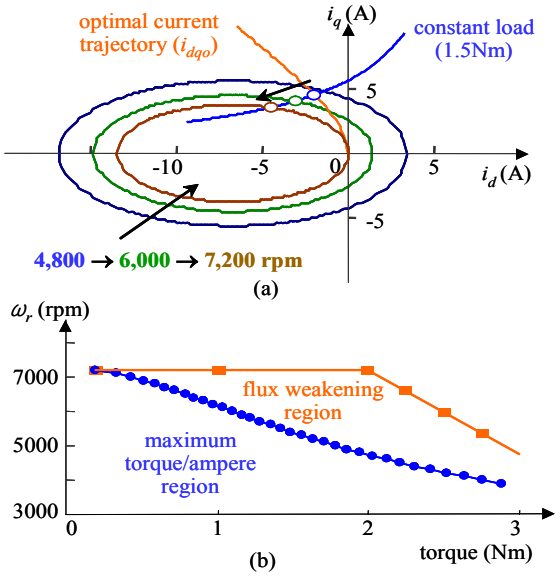

Fig. 6 Current trajectory for flux weakening
(a) Current trajectory with motor speed
(b) Operating region

Fig 7 shows a block diagram of the speed control and current control including maximum torque/ampere operation and flux weakening control.

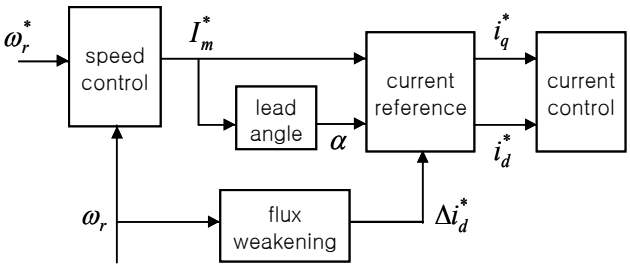

Fig. 7 Speed and current control

2.3 Compensation of torque pulsation

As shown in Fig. 1, the single piston rotary compressor has large torque pulsations in one revolution. This torque pulsation may be filtered and it does not make serious mechanical vibrations at high speeds. At low speeds, however, it causes serious mechanical vibrations of low frequencies so that it has problems in reliability. Such problems include frequent cracks in pipes connected to the accumulator of the compressor. Therefore, reduction of mechanical vibration is essential for low speed operation. The shape of the torque pulsation of a single piston rotary compressor is approximated in Fig. 1. Speed ripple, i.e., mechanical vibration, can be reduced by compensating the torque pulsations in one mechanical revolution. Direct torque control may be the best way to reduce mechanical vibrations, but it has some problems in calculating exact load torques due to errors of the estimated rotor position and the variations of torque constant with temperature variation. Therefore, in this paper, a feed-forward compensation of torque pulsation is applied. Information on torque pulsation shape and mechanical rotor position is required in order to compensate torque and to cancel torque pulsations. To simplify the shape of the compensated torque, a rectangular shaped feed-forward torque is applied in this paper. The duty ratio of the compensated torque is 50% of one revolution and the upper value of the compensated torque is about 170% of the average torque. Through the experiment, it is noted that the mechanical vibration for the two methods have similar characteristics.

3. Experimental Results and Discussion

Fig. 8 shows a block diagram of the proposed sensorless control algorithm. The speed error between the reference speed and estimated speed generates the γ-axis and δ-axis current reference for maximum torque/ampere operation. At high speeds, the negative γ-axis and δ-axis currents are added to the current reference by a flux weakening control. To compensate the torque pulsation at low speeds, the compensating torque is feed-forwarded to the current reference. The γ-axis and δ-axis reference currents are compared with γ-axis and δ-axis currents transformed from *abc* currents based on the estimated rotor position. A proportional-integral (PI) with decoupling current controller generates γ-axis and δ-axis voltage references.

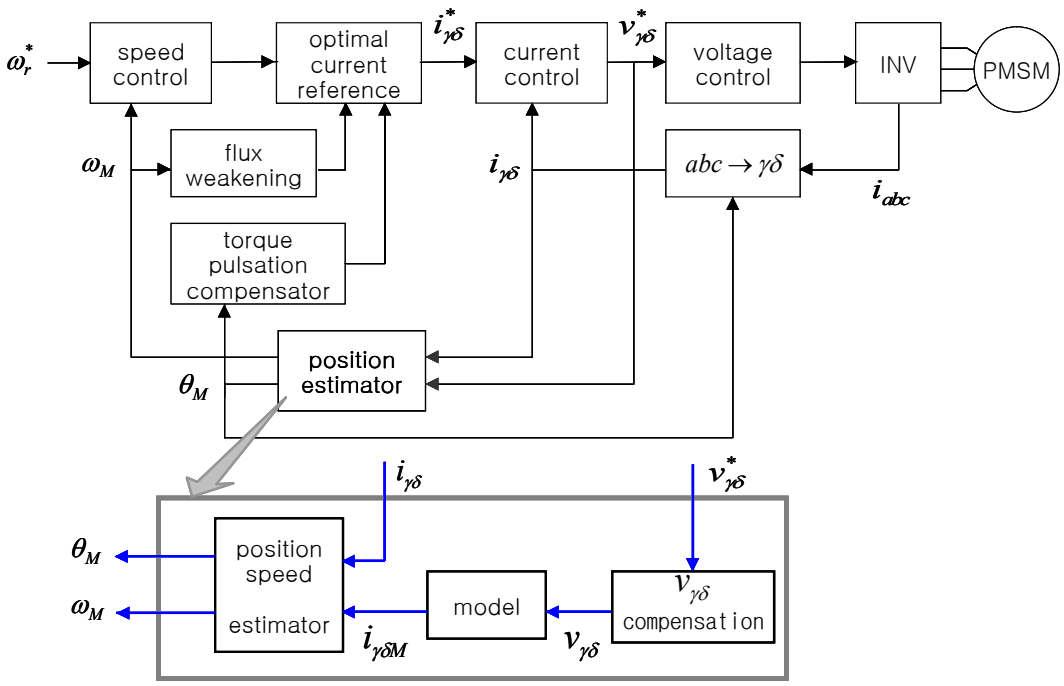

Fig. 8 Block diagram of sensorless control

Additionally, three phase voltages are applied to the motor through the space vector PWM. The PWM frequency of the space vector PWM is 4 kHz. The rotor position and speed are estimated by the position estimator by comparing γ-axis and δ-axis currents of the real system and model of the estimator. The γ-axis and δ-axis voltages of the estimator may be calculated from γ-axis and δ-axis reference voltages by considering the DC link capacitor voltage, turn-on and turn-off time, and dead time of the switching devices. The dead time depends on the switching status and current flow direction as well as the current level flowing in the switching devices. The sensorless control algorithm with the rotor position estimator is implemented by DSP, TMS320C2402.

Fig. 9 shows the real and estimated rotor position for constant dynamo loads. The load torque is 1.5Nm, which corresponds to the rated load of the set operating conditions. The estimated rotor position is able to track the real rotor position at low speeds and high speeds.

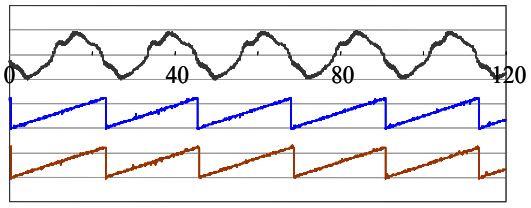

(a) 900 rpm

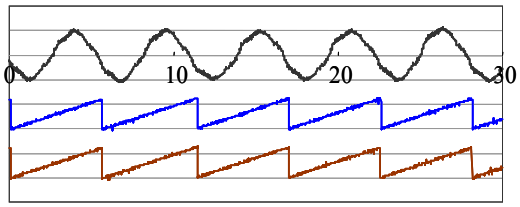

(b) 3,600 rpm

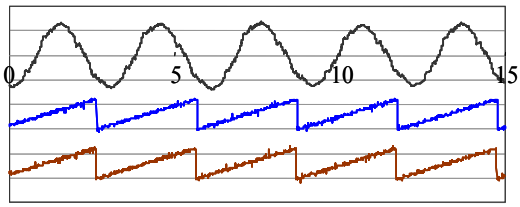

(c) 6,000 rpm

Fig. 9 Real and estimated rotor position for T_L = 15kgfcm
top : phase current (5A/div.)
middle : real rotor position (300deg/div.)
bottom : estimated rotor position (300deg/div.)

Concentrated windings in PM synchronous motors have larger back-EMF harmonic components compared with distributed windings. In this application, 5th and 7th back-EMF harmonics are, respectively, 12.0% and 2.5% of the fundamental components. Thus the phase currents have some harmonic components which reduce the torque ripples cause by the non-sinusoidal back-EMFs.

Fig. 10 shows speed ripples and currents at 900 rpm without and with torque compensation. Similar waveforms at 1,800 rpm are shown in Fig. 11. Without torque compensation, the peak to peak speed ripples at 900 rpm and 1,800 rpm are 250 rpm and 230 rpm, respectively. Those using the proposed algorithm with torque compensation are 100 rpm and 50 rpm, respectively.

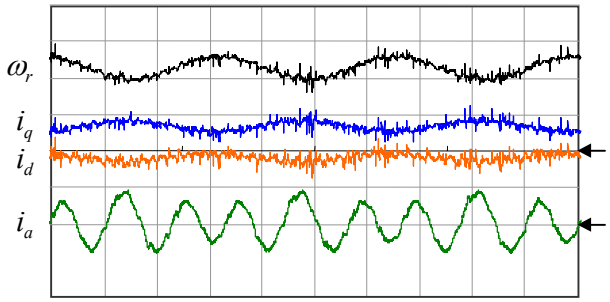

(a) Without torque compensation

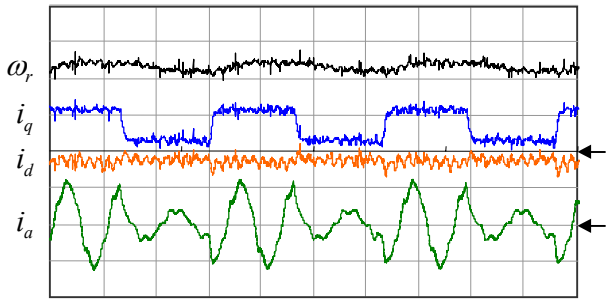

(b) With torque compensation

Fig. 10 Speed ripple and currents at 900 rpm
y-axis, speed: 400rpm/div., current: 5A/div.
x-axis, time: 200msec/div.

Large fluctuation in the phase current reduces torque ripples. Periods of large current flow correspond with compression periods of the refrigerant, as shown in Fig. 1, where large torque is required. One cycle of rectangular δ-axis current corresponds to 3 cycles of the phase current because the rotor has 6 poles.

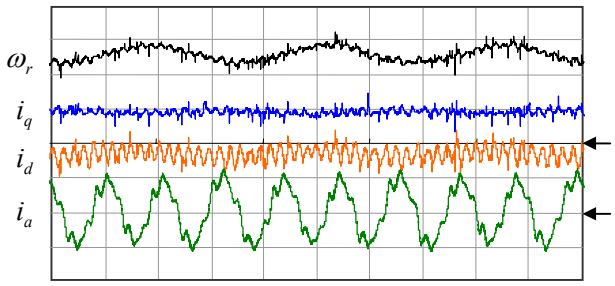

(a) Without torque compensation

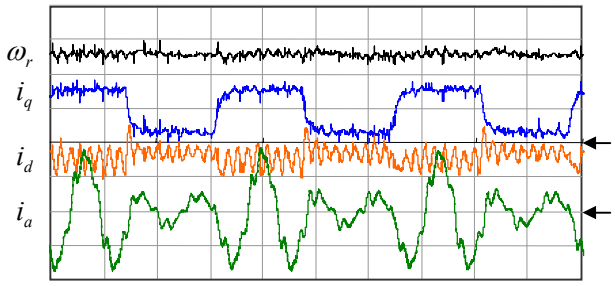

(b) With torque compensation

Fig. 11 Speed ripple and currents at 1,800 rpm
y-axis, speed: 400rpm/div., current: 5A/div.
x-axis, time: 100msec/div

Fig. 12 shows the mechanical vibration of the compressor with and without torque compensation. As mentioned in Fig. 10 and Fig. 11, large speed ripples without torque compensation generates large mechanical vibrations. As the speed increases, the mechanical vibration decreases due to the filtering of torque pulsation by the mechanical system so that the two methods have similar mechanical vibrations. Therefore, compensating torque pulsations is effective at low speeds, below 3,000 rpm. It is noted that if the compensated torque tracks the real pulsating torque, the torque ripple and the mechanical vibration can be reduced.

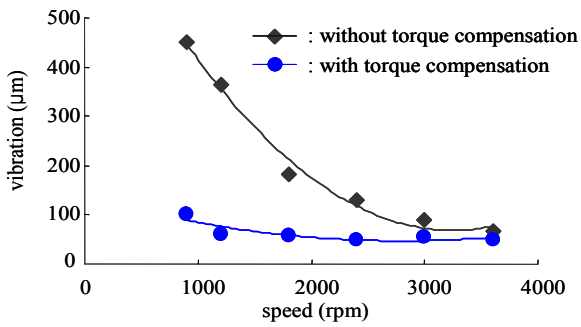

Fig. 12 Mechanical vibration of the compressor

In this case, a precise load torque observer is required, that is insensitive to errors of the estimated rotor position and to variations of torque with temperature fluctuations. In addition, the peak values of the phase currents will be larger, so higher power ratings of the inverter switches are required.

4. Conclusions

A sensorless control for an interior PM synchronous motor in a single-piston rotary compressor is presented. The rotor position is estimated by comparing the current errors between real currents and model currents of the position estimator. The pulsating torque of the single piston rotary compressor is compensated so that mechanical vibration is considerably reduced at low speeds. A flux weakening control with negative *d*-axis current provides high speed operation for rapid air cooling and heating in heat pump air-conditioners.

Appendix

Specifications of PM synchronous motors.

Rated power (P_{rated})	: 1Hp
Rated speed (ω_{rated})	: 3,600rpm
Number of poles (P)	: 6
Stator resistance (R_s)	: 0.58Ω
d-axis inductance (L_d)	: 9.0mH
q-axis inductance (L_q)	: 17.7mH
Back emf constant (ϕ_f)	: 0.0658Vsec.

Acknowledgment

This research was supported by Chungju National University - Scientific Research Fund (2005).

References

[1] F. Magnussen and C. Sadarangani, "Winding factors and Joule losses of permanent magnet machines with concentrated windings," in *Electric Machines and Drives Conference*, Vol. 1, pp. 333 – 339, June 2003.

[2] M.F. Rahman, M. E. Haque, L. Zhong and M. Nagrial, "A sensorless speed estimator for the direct torque control of

an interior permanent magnet synchronous motor drive," in *International Conf. on Power Electronics, Machines and Drives*, pp. 504 –509, June 2002.

[3] T. Aihara, A. Toba, T. Yanase, A. Mashimo and K. Endo, "Sensorless torque control of salient-pole synchronous motor at zero-speed operation," *IEEE Trans. Power Electronics*, Vol. 14, No. 1, pp. 202 – 208, Jan. 1999.

[4] J. P. Johnson, M. Ehsani and Y. Guzelgunler, "Review of sensorless methods for brushless DC," in *Conf. Rec. IEEE-IAS Annual Meeting*, pp. 143-150, 1999.

[5] N. Matsui, "Sensorless PM Brushless DC Motor Drives," *IEEE Trans. Industrial Electronics*, Vol. 43, No. 2, pp. 300-308, 1996.

[6] S. Kim and S. Sul, "High performance PMSM drives without rotational position sensors using reduced order observer," in *Conf. Rec. IEEE-IAS Annual Meeting*, pp. 75-82. 1995.

[7] K. Y. Cho, S. B. Yang and C. H. Hong, "Sensorless control of a PM synchronous motor for direct drive washer without rotor position sensors," *IEE Proc. Electrical Power Applications*, Vol. 151, No. 1, pp. 61-69, 2004.

Kwan-Yuhl Cho received his B.S. degree in Electrical Engineering from Seoul National University, Seoul, Korea, in 1986, and his M.S. and Ph.D. degrees in Electrical Engineering from the Korea Institute of Science and Technology (KAIST), Daejon, Korea, in 1988 and 1993, respectively. He worked for LG Electronics, Digital Appliance Research Lab., from 1986 to 2004. Since 2004, he has been with the Department of Information and Control Engineering at Chungju National University, Korea. His research interests are in the areas of variable speed motor drives and power converters. He is a member of the Korean Institute of Power Electronics (KIPE) and Korean Institute of Electrical Engineers (KIEE).